6-8October 2010, Barcelona, Spain

Heat Transfer Enhancement in High-Power Heat Sinks using Active Reed Technology

Pablo Hidalgo, Florian Herrault, Ari Glezer and Mark Allen
Georgia Institute of Technology, AtlantaGA30332-0405USA

Scott Kaslusky and Brian St. Rock
United Technologies Research Center, East Hartford, CT06108, USA

***Abstract*–Enhanced heat transfer in a high aspect ratio channel that models a segment of a novel, high-performance air-cooled heat-exchanger system for high-power electronics is characterized. Two innovative features that enable this system are integration of a centrifugal blower-diffuser with a high-density finned heat-sink, and microfabricated active reed elements that provide small-scale heat transfer enhancement at the reduced air flow rates. The present investigation focuses on the heat transfer and fluid mechanics that are associated with the small-scale motions induced by a piezoelectric vibrating reed that is integrated within a mm-scale channel. These time-periodic small-scale motions enhance convective heat transfer at the channel surfaces and the mixing of the thermal boundary layers with the core flow. High-magnification particle image velocimetry (PIV) measurements are used to characterize the interaction of the vortical structures shed by the reed with the channel wall and the induced small-scale motions. Performance enhancement by reed actuation is quantified in terms of increased power dissipation over a range of flow rates compared to the baseline flow in the absence of the reed. It is demonstrated that the channel's coefficient of performance can be increased by a factor of 1.4 while accounting for the power to the reed and the changes in channel pressure drop.**

I. INTRODUCTION

Modern, high-power heat sinks are characterized by highly-compact designs as shown, for example, in Fig. 1. In this configuration, a centrifugal blower-diffuser is integrated with a finned heat sink for high fin density. In this design, the heat sink fins form diffuser channels and additional splitter fins are introduced as the flow diffuses radially outward to maximize heat transfer area and enhance convective heat transport. Ambient air enters the centrifugal blower through a venturi that also serves as a hollow shaft for the blower motor, and the air flow through the blower and is directed through the curved diffuser channels. However, as in most compact high power heat sink designs forced convection heat transfer within the high aspect ratio fin channels is typically limited by the available air volume flow rate and consequently by the low channel Reynolds number. This limitation is manifested by two closely coupled stages of heat transport. First, the local heat transfer from the fin surface is limited by the temperature gradient within a thin thermal boundary layer. Second, the overall heat transport for a given mass flow rate is governed by the average temperature rise of the core flow. These deficiencies are commonly overcome by increased volume flow rate with significant concomitant increase in the required blower power.

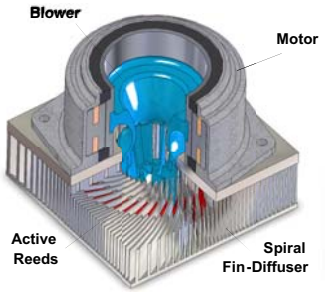

Fig. 1.High-power heat sink with integrated blower, diffuser and active reeds for enhanced heat transfer.

Enhanced local and global heat transport within the heat sink channels at higher flow rates (or channel Reynolds numbers) are typically associated with cross flow mixing that is induced the presence of unsteady, small-scale motions. The present work focuses on active enhancement of the heat transfer within the heat sink channels by deliberately inducing small-scale motions within the core flow at low channel Reynolds numbers. The presence of these small-scale flow motions disrupts the momentum and thermal boundary layers and enhances thermal mixing within the core flow, thereby significantly decreases the fin-to-air heat transfer resistance. In the present experiments, controlled, small-scale motions are induced by the time-periodic motion of miniature piezoelectric cantilever vibrating reeds that are placed within the mm-scale heat sink channels so that their planform surfaces are parallel to the channel walls (as shown schematically in Fig. 2). The reeds are driven at resonance and the period of the actuation frequency is smaller than the characteristic time of flight through the channel. The pressure drop that is caused by the presence of the reeds within the flow channels can be partially offset by the thrust produced by the reed. The motion of the reed blade induces time-periodic shedding of organized vortical structures (as shown schematically in Fig. 2) and turbulent-like small-scale flow motions that would

 ISBN: 978-2-35500-012-6

normally be present at much higher Reynolds numbers. These small-scale motions enhance the heat transfer coefficient at the fin surfaces as well as mixing of this heated air with the core channel flow to overcome the local and global limits of forced convective heat transport in the baseline channel in the absence of the reed. Intrafin vibrating reeds are attractive for integration in heat sinks because of their low form factor, low power requirements, and microfabrication compatibility.

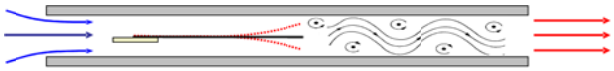

Fig. 2. Schematic rendition of the flow within a channel cooled by a vibrating reed.

The effectiveness of induced small scale motions for enhanced heat transfer in low-Reynolds number flows, that are characteristic of air cooling applications, was originally demonstrated using synthetic jet actuators (e.g., by direct impingement, Kercher et al. [1] and Pavlova et al. [2], or by integration with a heat sink, Mahalingam and Glezer [3],Gerty et al. [4-5], and Kota et al. [6]).The utility of piezoelectrically vibrating reeds for external cooling of low-power electronic packages (e.g., for notebook computers or cell phones) was investigated by Açikalin et al. [7] and Açikalin et al.[8],who also noted the lower power consumption and reduced noise compared to external cooling by conventional fans. Açikalin et al. [7] investigated the cooling performance of a piezo-fan on a heat sink used in conventional cell phones and laptop computers and reported better than 100% enhancement of the heat transfer coefficient compared to natural convection. In cooling of notebook computers, piezo-fans were effective in alleviating "hot spot" areas that were not adequately cooled by the system's conventional fan. In a later experimental and numerical investigation, Açikalin et al. [8] considered the thermal performance enhancement by a the jet-like streaming motion of a piezo-fan operated next to a constant heat flux source compared to natural convection cooling. The authors reported the sensitivity of the thermal performance to frequency deviation from the piezo-fan's resonance frequency, the distance from the heat source, and the oscillation amplitude (which depends on the blade length). DOE analysis showed an enhancement of the convective heat transfer coefficient of up to 275%. In an experimental and numerical investigation of the cooling characteristics of piezoelectric fans Wait et al. [9] showed that the flow associated with higher resonance modes can lead to enhanced mixing and improved cooling at the expense of significantly higher power consumption. Finally, Gerty [10] investigated small-scale heat transfer enhancement by a reed that is integrated within a heated channel. This work demonstrated the effectiveness of this approach for cooling of compact electronic packages in the absence and presence of a core flow and motivated the present work.

II. EXPERIMENTAL SETUP

The present investigation is conducted in a modular, high aspect ratio channel test section measuring 2.5 x 27.4 x 60 mm. The test section is preceded by a 260 mm long settling section having the same cross section, and an upstream contraction (contraction ratio of 28) to ensure fully-developed, spanwise-uniform flow (Fig. 3). The contraction section is driven by a regulated air supply monitored by a precision flow meter (the flow rate is measured to within 1.5%). The settling section is instrumented with multiple pressure ports along and around the flow channel. There are two interchangeable test sections. The first test section is designed for detailed measurements of pressure distributions while the second test section includes removable sidewalls that are integrated with heaters as shown in Fig. 4. To reduce blockage effects due to the reed, the side walls of the test section were designed with slight spanwise indentations (having a maximum depth of 460 μm on each side) opposite to the mounting post of the reed (cf. Fig. 5). Static pressure measurements within the test and settling sections were obtained using a high precision alcohol manometer coupled with a 48-port pressure switch. Fig. 3 shows a CAD model of the assembled test bed including the inlet contraction, settling section, and test section, and a section of the test section that was used for pressure measurements.

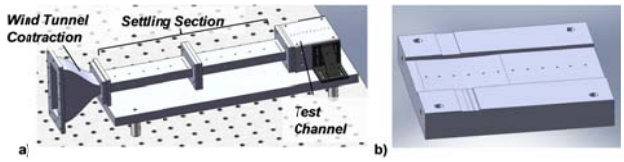

Fig. 3. a) Channel test set up assembly, and b) side wall of the test section for pressure measurements showing the mounting slots for the reed post and the spanwise indentation for alleviation of blockage.

The test section that is used for heat transfer measurements is shown in Fig. 4. The heater side walls are each comprised of microfabricated spanwise copper serpentine trace (having characteristic resistance of 40Ω) that is deposited on a silicon plates. Each individual heater is controlled using a high precision current source allowing resolution of the power dissipation to within20 mW. Individual spanwise windings of the serpentine heater are tapped for (spanwise-averaged) temperature measurements (with resolution that is better than 0.1°C) using the Joule heating of the copper windings. Each channel side wall consists of two adjacent silicon heater plates each measuring 42.4 x 30.41mm. The heaters are mounted on a ceramic frame with a sealed air gap on the backside of the frame for thermal insulation (only one heater is shown in Fig. 4 for clarity). The width of the channel is set by placing pairs of polycarbonate spacers that form the top and bottom walls of the channel and allow for rapid assembly and disassembly. The spacer pairs are used to clamp the reed mounting frame at the top and bottom ends of the channel using a machined recess (in the present configuration, the upstream end of the reed is 10 mm downstream of the channel inlet). Once the channel was assembled and attached to the settling section,

 ISBN: 978-2-35500-012-6

the entire test section was thermally insulated using fiberglass wool.

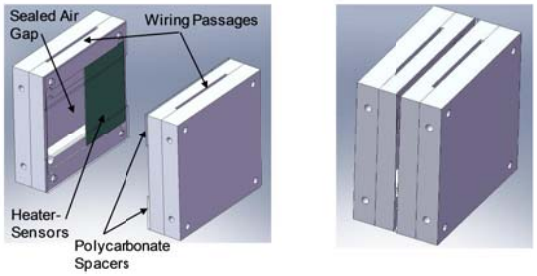

Fig. 4. CAD drawings of the exploded and assembled views of the heat transfer channel.

The piezoelectric reed used in the present experiments (Fig. 5) is 19 mm long and 25 mm wide and include a 100 μm thick plastic blade. The 127 μm thick PZT plate covered nearly 50% of the length of the plastic blade and the actuator is mounted on a 229 μm stainless steel post support. The resonance frequency of the reed is approximately 850Hz and its maximum peak-to-peak tip displacement is 1.4 mm (approximately 60% of the channel width).

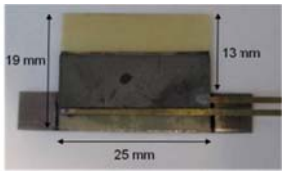

Fig. 5. The piezoelectric reed

IV. HEAT TRASNFER MEASUREMENTS

The cooling performance of the reeds is evaluated using two sets of measurements. In the first set, the power to the side wall heaters is invariant over a range of flow rates, and the heat transfer within the channel is assessed for the baseline flow in the absence of the reed, and then in the presence of the active reed. Reed activation results in a reduction in the wall temperature (compared to the baseline flow) and the measured differences in the wall temperature yields the local heat transfer enhancement. The second set of measurements is used quantify the increment in heat dissipation that can be achieved in the presence of the reed. Two comparisons are made. First, for a given channel flow rate, the dissipated heater power in the presence of reed actuation is increased until the channel wall temperature is approximately equal to the wall temperature of the baseline flow (in the absence of the reed). Second, for increased heat dissipation in the presence of reed actuation for a given flow rate, the flow rate of the baseline configuration is increased until the power dissipation matches the reed-enhanced dissipation at the lower flow rate.

As noted above, the first set of heat transfer experiments are conducted using invariant heat dissipation (12W) for several flow rates. The streamwise variation of heat transfer enhancement is shown in Fig. 6 in terms of the variation of the ratio of the Nusselt numbers $\eta = Nu_{\text{REED ON}}/Nu_{\text{REED OFF}}$ with distance from the tip of the reed (normalized by the channel width w). This figure demonstrates the importance of thermal spreading within the walls (or fins) substrate. The effects of spreading are evident in two salient features. First, the presence of the reed leads to a significant improvement in heat transfer coefficient (HTC) and a decrease in the wall temperature upstream of the reed. The second (and perhaps more important) effect is the domain of influence of the reed owing the substrate conductivity of the silicon (150 W/m^{o}K). Both features are consequence of the Biot number of silicon (the ratio of the substrate conductive thermal resistance to the convective thermal resistance at the wall). The Biot number of the silicon heaters is 0.048, (for reference, an aluminum channel would have a Biot number of 0.03), and therefore the thermal characteristics of the channel walls are similar to the characteristics of conventional heat sinks.

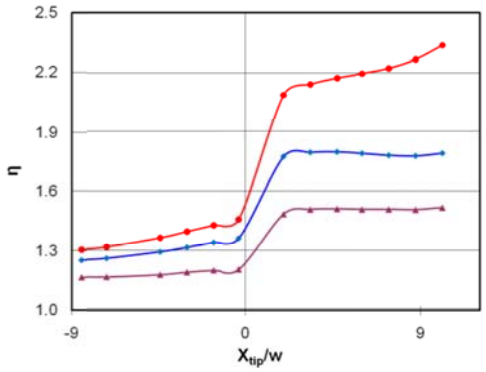

Fig. 6. Nusselt number enhancement at 30LPM (●), 40LPM (◆) and 75LPM (▲).

The variation of the channel pressure drop with flow rate and the streamwise variation of the static pressure are shown in Fig. 7a and b, respectively (in terms of the pressure coefficient $C_p = \Delta P/0.5 \cdot \rho_\infty \cdot V_\infty^2$). These data are shown for the baseline flow (in the absence of the reed), and in the presence of the active reed. Even though the channel walls are indented to alleviate blockage effects by the reed, there is still a significant increase in pressure drop (compared to the baseline flow) in the presence of the active reed. As shown in Fig. 7a, the increase in pressure drop diminishes with flow rate (it about 150% at 40 LPM and 80% at 75 LPM). As noted above, the reed blockage is caused by its maximum thickness which is approximately 20% of the width of the channel. The present work has demonstrated that wall indentation can significantly mitigate the increase in pressure drop and that the effectiveness of the indentation can be further improved by additional refinement. The streamwise variations of the static pressure within the channel at $Q = 60$ LPM in the absence and presence of actuation are shown in Fig. 7b. The pressure upstream of the reed tip (the tip is 29 mm downstream of the channel's inlet) is significantly higher than in the channel segment downstream of the tip due to blockage. While the actuation results in a small increase of the pressure upstream of the tip, downstream of the reed, the streamwise pressure gradient changes, and there

 ISBN: 978-2-35500-012-6

is a local increase in pressure. This rise in pressure downstream of the reed which is produced by thrust is not sufficient to overcome the pressure rise due to blockage.

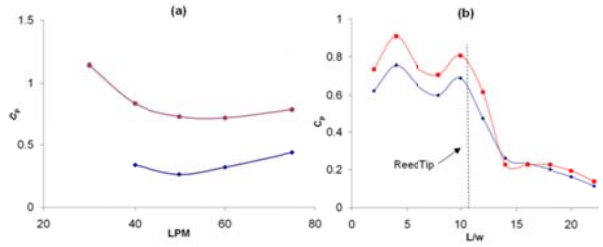

Fig. 7. a) Overall pressure drop in the baseline channel (◆)and in the indented channel with active reed (●); and b)Streamwise variation of static pressure along the indented channel at 60LPM with(■) and without (◆) reed actuation

The overall thermal enhancement by the reed in the flow channel is characterized in terms of several primary parameters including: the "fluid power" ($P_{fluid} = Q \cdot \Delta P$), the reed power (which is held invariant at 20 mW), the "total fluid power" φ (fluid power plus reed power) and the average HTC (Table I). These results show that for a given dissipated power (12 W) the HTC at $Q = 30$ LPM with reed actuation (about 160 W/m^2 ^{o}K) is comparable to the HTC of the baseline flow at over twice the flow rate ($Q = 75$ LPM). This is noteworthy because the total flow and reed power at $Q = 30$ LPM is 38 mW while the flow power at $Q = 75$ LPM is 110 mW or nearly 2.9 times higher. Furthermore, preliminary observations indicate that a reduction of 25% in reed power results in a trivial loss in cooling effectiveness, but can save 13% of the total "flow power" at $Q = 30$ LPM.

TABLE I
RESULTS SUMMARY HEAT TRANSFER AND POWER INPUT TEST

LPM	Reed Mode	Heaters Power (W)	Fluid Power (mW)	Reed Power (mW)	Total Power (mW)	Avg. HTC (W/m^{2}K)
30	Off	12	8	0	8	83
	On	12	18	20	38	171
40	Off	12	13	0	13	93
	On	12	32	20	52	167
60	Off	12	41	0	41	120
	On	12	198	20	218	253
75	Off	12	110	0	110	160
	On	12	198	20	218	253

Thermal enhancement is also measured by comparing the thermal performance at equal total fluid power for the baseline flow and in the presence of the active actuator. In Table II the thermal performance of two flows that have approximately the same "total fluid power" is compared. The total fluid power at $Q = 30$ LPM with active reed (38 mw) is almost the same as at $Q = 60$ LPM in the absence of the reed (i.e., the baseline flow, 41 mW). For these operating conditions, the average HTC increases by 42% with reed actuation *at half the flow rate*. As shown in Fig. 8, the average thermal resistance (θ) of the actuated flow decreases by 21% (the maximum reduction in θ is 55%). These data indicate that for the same operating conditions the channel can be significantly lengthened with a comparable increase in the dissipated heat while keeping the reed power unchanged. Under these flow conditions, the pressure rise in a longer channel at $Q = 30$ LPM is four times lower than at 60 LPM (for a given channel cross section and working fluid $\Delta P \propto f Q^2 L$)

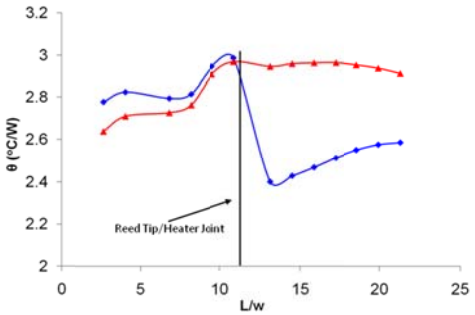

Fig. 8. Comparison of the thermal resistances of the baseline flow at 60LPM (▲) with a flow having similar total fluid power in the presence of an active reed at 30 LPM (◆).

TABLE II
RESULTS SUMMARY HEAT TRANSFER AND POWER INPUT TEST

LPM	Heaters Power (W)	Fluid Power (mW)	Reed Power (mW)	Total Power (mW)	Avg. HTC (W/m^{2}K)
30	12	18	20	38	171
60	12	41	0	41	120

For the two flow conditions shown in Table II (i.e., similar total flow power in the presence of an active reed at $Q = 30$ LPM, and for the baseline flow at $Q = 60$ LPM), the wall temperature T when the reed is active is lower than for the baseline flow at a higher flow rate. It is therefore desirable to determine by how much the dissipated power in the actuated flow at $Q = 30$ LPM can be increased to reach a wall temperature that is similar to that of the baseline flow at $Q = 60$ LPM. Fig. 9 shows that the nominal difference in wall temperature between the two flows is approximately 6^{o}C. In order to (approximately) equalize the wall temperatures between the two flows, the dissipated power is increased by about 25% to almost 15 W. These measurements are conducted over a range of flow rates in the presence of reed actuation such that the wall temperature matches the corresponding baseline wall temperature. It is found that the dissipated heat can be increased up to 20 W at 30 LPM, 19W at 40 LPM, 18W at 60 LPM and 17W at 75 LPM, which correspond to increases of 66%, 58%, 50% and 42%, in dissipated heat, respectively.

The variation of the thermal resistance θ of the channel with total fluid power φ is computed for the several flow rates of the baseline flow and with reed actuation (Fig. 10). In the absence of actuation $\theta \propto \varphi^{-0.27}$. When the actuation is applied $\theta \propto \varphi^{-0.33}$ and there is a clear offset that indicates a decrease in the thermal resistance and an increase in fluid power. As noted above, the increase in fluid power can be mitigated by adjusting the wall indentation and therefore, it should be possible to realize a channel configuration with an integrated reed that decreases the thermal resistance of the system without a significant increase in total fluid power

 ISBN: 978-2-35500-012-6

investment. Furthermore, as noted in the discussion in connection with Fig. 9, reed actuation enables significantly higher heat dissipation at the same total fluid power than the baseline flow at significantly higher flow rates.

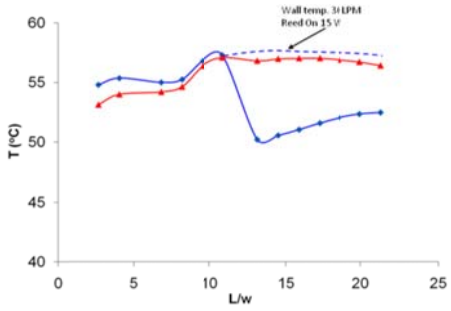

Fig. 9. Streamwise variation of the wall temperatures of the reed enhanced flow at 30 LPM (◆) and of the baseline channel at 60LPM (▲) for similar total fluid power.

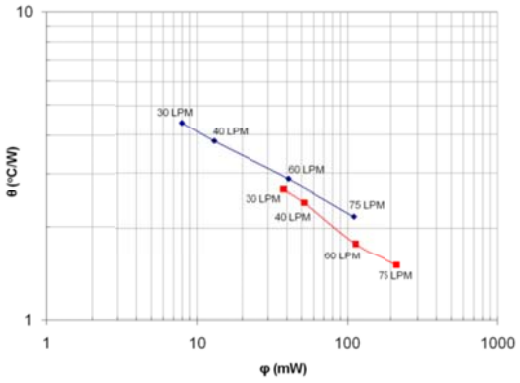

Fig. 10.Variation of thermal resistance with the total fluid power for several flow rates with (■) and without (◆)reed actuation.

Finally, the thermal enhancement that is enabled by reed actuation is quantified using the coefficient of performance (COP), which is the ratio of the dissipated heat and the total fluid power invested. Fig. 11 shows the variation of the COP of the channel with flow rate. Three measurement sets are considered. The first set is the variation of the COP for the baseline flow (in the absence of the reed) for constant heat dissipation (12 W). The second set is the corresponding COP with reed actuation where at each flow rate the dissipated heat is increased until the surface temperature within the channel matches the temperature of the corresponding baseline flow. Finally, the third set of measurements compares the COP of the reed actuated flow at $Q = 30$ LPM while dissipating 20W to the COP of the baseline flow for which the flow rate is increased until the heat dissipation is also 20 W at the same wall temperature as for the reed-actuated flow at 30 LPM. These heat dissipation conditions are matched (in terms of the channel's wall temperature) at $Q = 72$ LPM. It is important to note that under these matched thermal dissipation conditions the COP of the reed actuated flow is 535 while the corresponding COP of the baseline flow is 220 which is 1.4 times less efficient than the reed-enhanced configuration. The COP is inversely proportional to and clearly sensitive to the total fluid power.

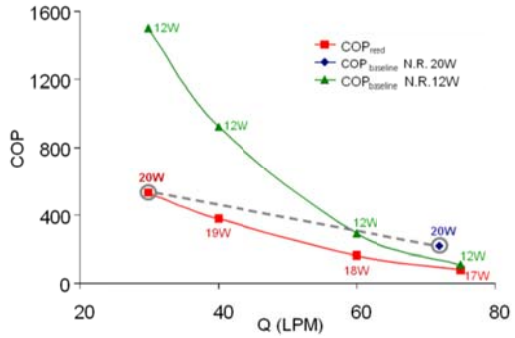

Fig. 11. Variation of the COP with volume flow rate for the baseline channel for a power dissipation of 12W (▲), 20W (◆) and the reed-enhanced channel at a wall temperatures that are approximately equal to the baseline channel for each flow rate (■).

V. PIV MEASUREMENTS

The flow field in the cross stream center-span ($z = 0$) plane within the channel is measured at 30 LPM ($Re_w = 2200$) using high magnification particle image velocimetry in the baseline flow and in the presence of the active reed. The measurement domain extends 4 channel widths (10 mm) downstream of the tip of the reed and the magnification is 3μm/pixel. The effect of the reed on the flow is demonstrated using phase-averaged cross stream distributions of spanwise vorticity concentrations and velocity vectors at two phases during the motion of the reed (having period T) as shown in Fig. 12. At $t = 0$ and $0.583T$ the tip of the reed is 0.47 mm above (Fig. 12a) and 0.125 mm below (Fig. 12b) the channel's centerline. These distributions show the CW (red) and CCW (blue) vorticity concentrations that are advected past the reed's blade (above and below the centerline) along with the corresponding vorticity concentrations within the boundary layers on the top and bottom surfaces. These images also show the induced changes in the speed of the core flow as the reed moves closer to and ways from the channel walls. Perhaps the most salient feature of these data is the clear evidence of the time-periodic disruption of the flow within the wall boundary layers indicating enhanced heat transfer and mixing with the cooler core flow. The time-periodic motions that are induced by the reed lead to the formation and shedding of counter rotating vortical structures that interact with and disrupt the boundary layers on the channel's walls. Fig. 13a and b are cross stream maps of time-averaged turbulent kinetic energy (TKE) within the same streamwise domain in the absence and presence of actuation. In the absence of actuation (Fig. 13a), the TKE is relatively low (considering the channel Reynolds number). However, when the reed is actuated (Fig. 13b) there is a remarkable enhancement in TKE which is indicative of enhanced small-scale motions within the channel and therefore strong mixing with the core flow.

 ISBN: 978-2-35500-012-6

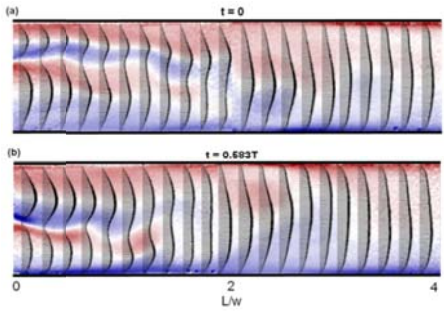

Fig. 12.Phase-locked PIV measurements of cross stream velocity and spanwise vorticity concentrations downstream of the vibrating reed.

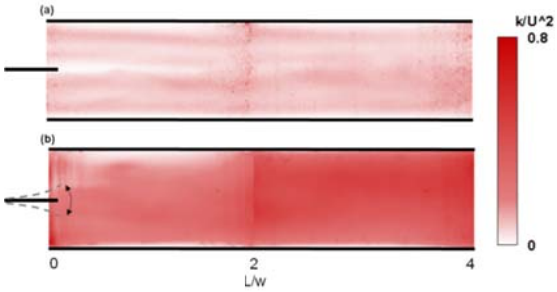

Fig. 13. Time-averaged TKE in the absence (a) and presence (b) of reed actuation for volume flow rate of 30LPM.

VI. Conclusions

The present experimental investigation focuses on heat transfer enhancement within a mm-scale straight channel that is characteristic of the low-Reynolds number flows within high-power heat sink channels. Active enhancement of the heat transfer within the heat sink channels is effected by induced small-scale motions that disrupt the momentum and thermal boundary layers and enhances thermal mixing within the channel's core flow, thereby significantly decreasing the fin-to-air heat transfer resistance. These motions are induced by the time-periodic motion of miniature piezoelectric cantilever vibrating reeds that are placed within the channel so that their planform surfaces are parallel to the channel walls and the actuation period is smaller than the characteristic time of flight through the channel.

Comparisons between the baseline flow (in the absence of the reed) and in the presence of actuation show that at the same total fluid power investment, actuation results in a 42% increase in heat transfer coefficient at about half the flow rate. Furthermore, comparisons of the two flows at a given power dissipation show that in order to achieve similar heat transfer coefficient the total fluid power investment in the baseline flow has to be nearly 2.9 times higher. Furthermore, for the same wall temperature in the two flows, the coefficient of performance (COP) in the presence of actuation is approximately 1.4 times higher than in the baseline flow. The present results indicate that the reed technology has the potential to significantly enhance the efficiency of conventional, high-power heat sinks without increasing their cooling volume flow rate or fin density.

ACKNOWLEDGMENT

This work was supported by DARPA's Microsystems Technology Office (MTO) MACE program.

REFERENCES

[1] D.S. Kercher, J. Lee, O. Brand, M. G. Allen and A. Glezer, "Microjet Cooling Devices for Thermal Management of Electronics," IEEE Transactions on Components and Packaging Technologies, vol. 26, No.2, pp.359-366, 2003.

[2] A. Pavlova and M. Amitay, "Electronic cooling using synthetic jet impingement," Journal of Heat Transfer, vol. 128, pp.897-907, 2006.

[3] R. Mahalingam and A. Glezer, "Design and thermal characteristics of a synthetic jet ejector heat sink," Journal of Electronic Packaging, vol. 127, pp.172-177, 2005.

[4] Gerty, D., Mahalingam, R., et al. (2006). "Design and Characterization of a Heat Sink Cooled by an Integrated Synthetic Jet Matrix." Proceedings of ITHERM 2006, May 30-June 2, 2006, San Diego, CA.

[5] D. Gerty, D.W. Gerlach, Y.K. Joshi and A. Glezer, "Development of a prototype thermal management solution for 3-D stacked chip electronics by intervealed solid spreaders and synthetic jets," THERMINIC 2007, Budapest, Hungary, 17-19 September 2007.

[6] K. Kota, P. Hidalgo, Y.K. Joshi and A. Glezer, "Thermal management of a 3D chip stack using a liquid interface to a synthetic jet cooled spreader," THERMINIC 2009, Leuven, Belgium, 7-9 October 2009.

[7] T. Açikalin, S.M. Wait, S.V. Garimella and A. Raman, "Experimental investigation of the thermal performance of piezoelectric fans," Heat Transfer Engineering, vol. 25, pp. 4-14, 2004.

[8] T. Açikalin, S.V. Garimella, A. Raman and J. Petroski, "Characterization and optimization of the thermal performance of miniature piezoelectric fans,"Int. J. Heat and Fluid Flow vol. 28, pp.806-820, 2007.

[9] S.M. Wait, S. Basak, S.V. Garimella and A. Raman, "Piezoelectric fans using higher flexural modes for electronics cooling applications," IEEE Transactions on Components and Packaging Technologies, vol. 30, No.1, pp.119-128, 2007.

[10] D. Gerty, "Fluidic-driven Cooling of Electronic Hardware: Part I: Channel Integrated Vibrating Reed; Part II: Active Heat Sink," PhD Thesis, 2008.

 ISBN: 978-2-35500-012-6